

# High Radiation Effects on Different Performance of Solar Cells

Hammad Abozied mohammed<sup>1</sup> and Mohamed S. El\_Tokhy<sup>2</sup>

<sup>1</sup>*Elec. Eng. Department, Faculty of Engineering, Assiut University, Assiut, Egypt.*

<sup>2</sup>*Engineering Department, NRC, Atomic Energy Authority, Inshas,  
P. No. 13759, Cairo, Egypt.*

## Abstract

Recent interest has focused on implementation of solar cells where they are a clean renewable energy source. The primary source of this paper is to analyze the performance of solar cells under high radiation effects. Therefore, explicit and implicit models of solar cells characteristics are proposed. Matlab environment is used to device these models. The implicit models are a graphical user interface that is investigated by MATLAB Simulink. Moreover, the various effects of ionized radiation on solar cells characteristics are evaluated through parameters tuning. Hence, curves for photocurrent, output power, maximum output power and fill factor are presented with special emphasis on radiation effects. The solar cells under study are based on proposed four parameters electronic components. Also, comparison between the proposed mathematical and published results in literature are conducted and validated. The implemented models help designers and scientists to optimize the solar cells construction. Therefore, optimization of the output power per cell is of primary concern.

**Keywords:** Radiation Damage, Ionizing Radiation, P–N Junction, Electronic Circuit

## 1. INTRODUCTION

In developing countries like Egypt, the considerable fraction of the population suffers from the grid electricity and significant part of rural areas still has bad electricity service [1].

Egypt enjoys with excellent solar radiation. The annual global solar radiation is between 1900 and 2600 kW h/m<sup>2</sup> from north to south [2]. However, diesel generation has bad maintainability, unreliable fuel supply, and high generation cost. One method in order to overcome these problems is a concentrated photovoltaic (PV) system. It converts light energy into electrical energy. Photovoltaic cells are being employed for many applications such as remote area devices, space satellites, fission detectors [3] and solar-powered engines. However, the main applications of PV systems are in either stand-alone or grid connected configurations. Standalone PV generation systems are attractive as they are indispensable electricity source for remote areas. However, PV generation systems have two major problems:

- (i) Low conversion energy in low irradiation conditions
- (ii) The amount of electric power generated by PV arrays varies continuously with weather conditions [4].

Therefore, the use of photovoltaic cell for a better and intensive benefit of the renewable solar energy has been increased [5-6]. Moreover, the installation of PV generation systems is rapidly growing due to concerns related to the environment, global warming, energy security, technology improvements and decreasing costs. Furthermore, PV generation system is considered as a clean and environmental friendly source of energy. The advantages of using photovoltaic systems include low maintenance, ease of installation and reliability. However, the main obstacles for using solar energy are the high initial costs and the very low PV cell conversion efficiency. Moreover, the system efficiency depends on several factors such as solar radiation, ambient temperature and state of the solar panels [7]. Furthermore, the solar cells used in space environment are subjected to a bombardment of charged particles of a wide energy range [8-9]. This bombardment introduces defects in the constituent materials of the cells. Consequently, it deteriorates the electronic properties of the cell. The main sources of radiation that affecting on PV modules are; electrons trapped by the terrestrial magnetic field, protons coming from the sun and the particle flux depending on the orbit of the mission. Other sources of damage are neutrons and  $\gamma$ -rays [9]. This paper is organized as follows: Section 2 presents the models description and operational principle. In Section 3 we present proposed mathematical models. Section 7 introduces the obtained results and discussion. Section 7 is devoted to the conclusion of this work.

## **2. MODELS DESCRIPTION AND OPERATIONAL PRINCIPLE**

The solar spectrum at air mass ratio (AM) of 1.5 extends over wavelength range 0.3 – 2.5  $\mu\text{m}$ . therefore, the solar irradiations can't ionize gas atoms and molecules at the ground level at N.T.P. But, the cosmic ray energy ( $3 \times 10^{18} \text{eV}$ ) has bad effects on the solar cell structure. The effect of ionizing radiation on the physical properties of semiconductor devices was studied [10]. Ionizing radiation has two effects on solar cells. These are transient and permanent effects. The former is due to the electron-hole pair generation. However, the latter is due to the bombardment of a cell with

radiation which causes changes in the crystal lattice. Furthermore, it creates traps for charge carriers. Hence, the change in the reverse saturation current and the change in the forward voltage of the diode are a measure of the total integrated radiation.

A current is created in the circuit when p–n junction is subjected to ionizing radiation. The current is divided into a prompt component and a delayed component. The latter occurs at the same time as the ionization pulse. However, the former can continue well after the end of the ionization process [10]. A considerable amount of lattice damage is caused as well as radioactive particles enter the cell body. These defects act as recombination centers trapping for the generated carriers. Consequently, three phenomena occur. These are electron-hole pairs, Compton effect and electron-positron pair [11]. Solar cells are connected in series and in parallel in order to form the desired voltage and current levels. They remain the basic semiconductor components of a PV panel [12]. There are different kinds of parametric models presented in various literatures in the past few decades, like single-diode model, two diode model and three diode models. The most commonly used models are single diode and two diode model. Since, they provide better relations with a practical solar cell keeping in mind the simplicity in implantation and the iteration speed in the extracting parameters as well as I-V and P-V curves. Also, it gives minimum error with respect to characteristics of solar PV cell. The two diode model gives more precise characteristics close to practical photovoltaic solar cell as compared to single diode model characteristics. Also, the two diode model implementation has more complex equation with two more unknown parameters. However, the single diode model is better as it will save time [13]. The primary solar cell equivalent circuit contains a current source with a parallel diode and shunt resistance [14]. It is called single-diode model. However, the four-parameter model includes a photocurrent source, a parallel diode, parallel shunt resistance and a series resistor. These four parameters determination is difficult due to the exponential equation of p–n diode junction [14]. The equivalent circuit consists of a lumped series resistance and a diode as shown in Fig. 1. This circuit is widely used for analysis of solar cells. The series and shunt resistances can be considered to be parasitic circuit elements. It is introduced by the behavior of real solar cells with their technical limitations.

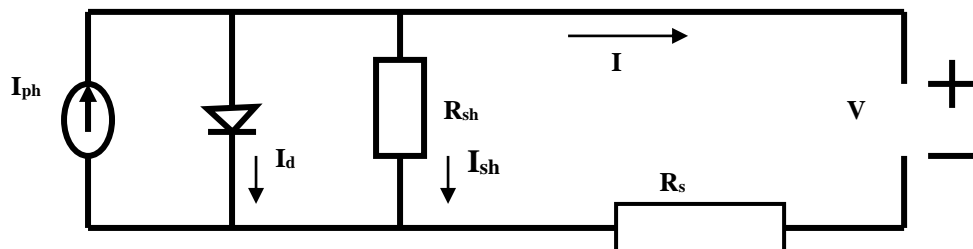


**Fig. 1** Equivalent circuit for photovoltaic solar cells and modules

### 3. PROPOSED MATHEMATICAL MODELS

#### 3.1 The induced photocurrent model

The temporal variation of free carrier concentration in the bulk is equal to the photo generation rate minus the spontaneous recombination rate and the recombination losses. Then, the rate equations describing the time evolution of concentration of carriers in the device when illuminated by a flux density of photons,  $\Phi(t, x)$ , are [15]

$$\frac{dn}{dt} = \alpha\phi(t, x) - \frac{n}{\tau_n} - Rnp \quad (1)$$

$$\frac{dp}{dt} = \alpha\phi(t, x) - \frac{p}{\tau_p} - Rnp \quad (2)$$

where  $p$ ,  $n$ ,  $\tau_n$ ,  $\tau_p$ ,  $R$ ,  $\alpha$ , and  $\Phi$  denote the density of holes, density of electrons, electron lifetime, holes lifetime, recombination rate, absorption coefficient, and incident photon flux density, respectively. Unfortunately, no solution to the rate equations (1-2) is known for the authors. However, a simple treatment for these equations (1-2) is illustrated in [14]. In this reference the illumination is assumed to be homogenous through the device. Therefore, the generation term,  $\alpha \Phi(t, x)$ , becomes independent of  $x$ , that yields  $\Phi(t, x) = \Phi(t)$ . For a Dirac input

$$\phi(t) = \phi_0 \delta(t) \quad (3)$$

Where  $\phi_0$  and  $\delta(t)$  denote initial incident photon-flux density and Dirac input, respectively.

Thus, the dynamical behavior of the device can be modeled by the following spatial independence rate equations [16]

$$\frac{dn}{dt} = \alpha\phi_0\delta(t) - \frac{n}{\tau_n} - Rnp \quad (4)$$

$$\frac{dp}{dt} = \alpha\phi_0\delta(t) - \frac{p}{\tau_p} - Rnp \quad (5)$$

We solved the above simultaneous equations (4-5) analytically. Hence, the carriers concentrations are obtained. Those are simplified as

$$n = (\alpha\phi_0 \text{heaviside}(t) + n_0 - \alpha\phi_0\xi) \exp\left(-\frac{1 + Rp_0\tau_n t}{\tau_n}\right) \quad (6)$$

$$p = (\alpha\phi_0 \text{heaviside}(t) + p_0 - \alpha\phi_0\xi) \exp\left(-\frac{1 + Rn_0\tau_p t}{\tau_p}\right) \quad (7)$$

The photocurrent across the device is given by

$$I = qES(\mu_n n + \mu_p p) \quad (8)$$

Where  $q$ ,  $\mu_n$ ,  $\mu_p$ ,  $S$  and  $E$  denote elementary charge, the mobility of electrons, the mobility of holes, device area and electric field reigning in the depletion layer, respectively.

A new formula for the photocurrent is deduced by substitution from Eqs. 6, 7 in Eq. 8. It can be expressed as follows:

$$I = qES \left( \left( \mu_n e^{-\frac{1+Rp_0\tau_{n,t}}{\tau_n}} + \mu_p e^{-\frac{1+Rn_0\tau_{p,t}}{\tau_p}} \right) (\alpha\phi_0 \text{heaviside}(t) - \alpha\phi_0\xi) + \left( n_0\mu_n e^{-\frac{1+Rp_0\tau_{n,t}}{\tau_n}} + p_0\mu_p e^{-\frac{1+Rn_0\tau_{p,t}}{\tau_p}} \right) \right) \quad (9)$$

This equation is the proposed photocurrent model. The parameters of this formula are tuned to study and evaluate the performance characteristics of the photocurrent.

### 3.2 Output power model

A solar cell can be considered as a black box which gives output current under light illumination. Electrons and vacancies move freely inside the box. The radiation-induced defects can affect the equilibrium concentration of carriers. The change in equilibrium concentration of minority carriers inside the black box should be a function of time under the irradiation of space energetic charged particles. This can be shown as follows [17]

$$\frac{dN^*}{dt} = -\frac{(N^* - \varphi)}{\theta} \quad (10)$$

$$I^* = \varphi + (1 - \varphi)e^{\left(\frac{-t}{\theta}\right)} \quad (11)$$

Where  $N^*$ ,  $\varphi$ ,  $\theta$ ,  $I^*$  and  $t$  denote the normalized equilibrium concentration of carriers, particles and target materials, the factor related with irradiation fluence, the normalized photo-induced current, and the irradiation time, respectively.

The authors try to solve the above equation (10) analytically in order to present a mathematical model. By solving Eq. 10 using the following boundary condition:

$$N^* = N_0 \text{ at } t=0 \quad (12)$$

Where  $N_0$  denotes the carrier concentration before irradiation, an equation for the normalized equilibrium concentration of carriers is deduced and rearranged as follows:

$$N^* = \varphi + e^{\left(\frac{-t}{\theta}\right)} (N_0 - \varphi) \quad (13)$$

Therefore, by solving Eq. 13 for  $\varphi$ , we obtain

$$\varphi = \frac{N_0 e^{\left(\frac{-t}{\theta}\right)}}{-1 + e^{\left(\frac{-t}{\theta}\right)}} \quad (14)$$

By substituting from Eq. 14 in Eq. 11, we get

$$I^* = \frac{N_0 e^{\left(\frac{-t}{\theta}\right)}}{-1 + e^{\left(\frac{-t}{\theta}\right)}} + \left(1 - \frac{N_0 e^{\left(\frac{-t}{\theta}\right)}}{-1 + e^{\left(\frac{-t}{\theta}\right)}}\right) e^{\left(\frac{-t}{\theta}\right)} \quad (15)$$

Thus, the current can be obtained by

$$I = I^* I_0 \quad (16)$$

Where  $I_0$  is the pristine photon induced current. A formula for the current is obtained by substitution from equation (15) in equation (16), an equation for the current can be obtained as follows

$$I = I_0 \left( \frac{N_0 e^{\left(\frac{-t}{\theta}\right)}}{-1 + e^{\left(\frac{-t}{\theta}\right)}} + \left(1 - \frac{N_0 e^{\left(\frac{-t}{\theta}\right)}}{-1 + e^{\left(\frac{-t}{\theta}\right)}}\right) e^{\left(\frac{-t}{\theta}\right)} \right) \quad (17)$$

However, the power is given by

$$P = IV \quad (18)$$

Therefore, by substitution from equation (17) in equation (18), a model for the radiated output power is deduced. This equation is modified and rearranged as:

$$P = I_0 \left( \frac{N_0 e^{\left(\frac{-t}{\theta}\right)}}{-1 + e^{\left(\frac{-t}{\theta}\right)}} + \left(1 - \frac{N_0 e^{\left(\frac{-t}{\theta}\right)}}{-1 + e^{\left(\frac{-t}{\theta}\right)}}\right) e^{\left(\frac{-t}{\theta}\right)} \right) V \quad (19)$$

This proposed mathematical model depends on analytical manipulation. However, this solution remains difficult for interpretation. Thus, an implicit solution using block diagram model for normalized power is presented as shown in Fig.2. This implicit solution based on numerical analysis. This illustrated the small variation between the introduced models results. Parameters tuning by implicit solution is the main strength of this study.

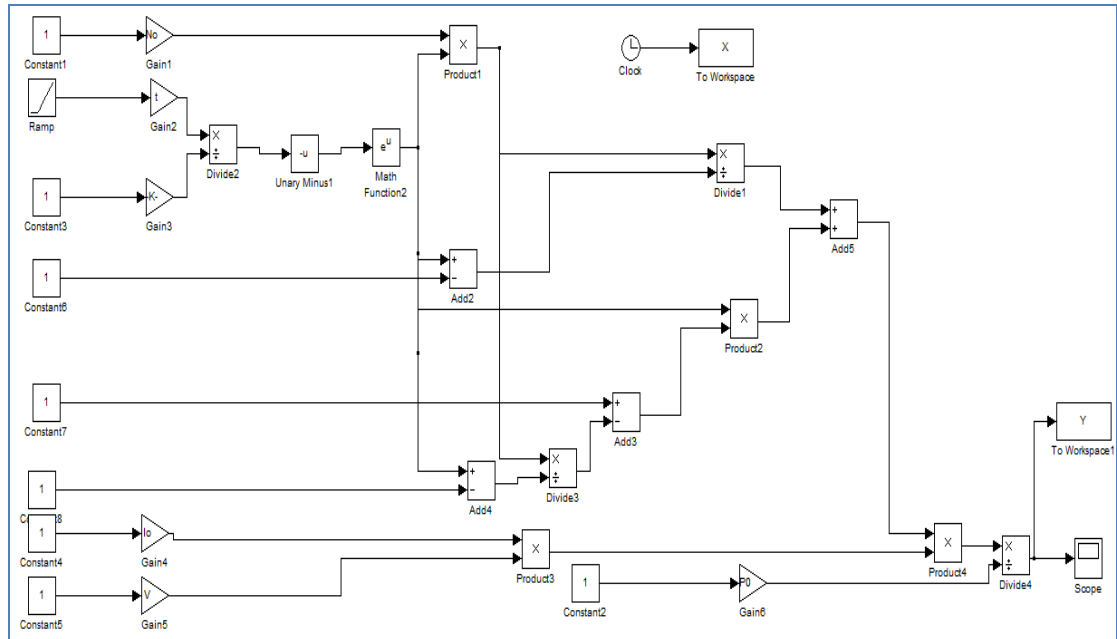


**Fig. (2)** The proposed block diagram model of normalized power

### 3.3 Maximum output power model

A photovoltaic array under uniform radiation presents a current–voltage characteristic with a single point that called Maximum Power Point (MPP). The output power from a photovoltaic array decreases significantly when current–voltage curves of solar modules are not identical due to shading. Shading panels greatly reduce system performance and output power has several maxima. However, tracking algorithms of the MPP are usually based on the assumption that power curve generated has a single peak [18].

The series resistance and the ideality factor are evaluated by means of linear relation between open circuit voltage conditions and inverse of short current intensity [19].

$$\frac{dV}{dI} = -\left( R_s + \frac{nV_T}{I_{sc}} \right) \tag{20}$$

Where  $n$ ,  $V$ ,  $V_T$ , and  $I_{sc}$  denote the ideality factor ( $>1$ ), mean cell voltage, thermodynamic voltage, and short-circuit current, respectively. By solving Eq. 20 using the boundary conditions,  $V=V_{oc}$  at  $I=0$ , we deduced

$$V = V_{oc} - IR_s - \frac{I}{I_{sh}} nV_T \tag{21}$$

Where  $V_{oc}$  denotes the open-circuit voltage. However, the following equation is obtained at the MPP

$$\frac{dP}{dI} = V + I \frac{dV}{dI} \quad (22)$$

By substituting Eqs. 20 and 21 in Eq. 22, we find

$$\frac{dP}{dI} = \left( V_{oc} - IR_s - \frac{I}{I_{sh}} nV_T \right) - I \left( R_s + \frac{nV_T}{I_{sc}} \right) \quad (23)$$

By integrating Eq. 23 as follows

$$\int_0^{P_{max}} dP = \int_0^{I_{max}} \left( \left( V_{oc} - IR_s - \frac{I}{I_{sh}} nV_T \right) - I \left( R_s + \frac{nV_T}{I_{sc}} \right) \right) dI \quad (24)$$

An equation for the maximum power was deduced and arranged as follows

$$P_{max} = - \left( R_s + \frac{nV_T}{I_{sh}} \right) I_{max}^2 + V_{oc} I_{max} \quad (25)$$

This mathematical handling of maximum power is based on explicit solution. The effect of varying parameters on maximum operation power by Eq. 25 is difficult to be considered. Hence, the block diagram model of maximum power by MATLAB Simulink is of primary concern. This implemented in Fig. 3.

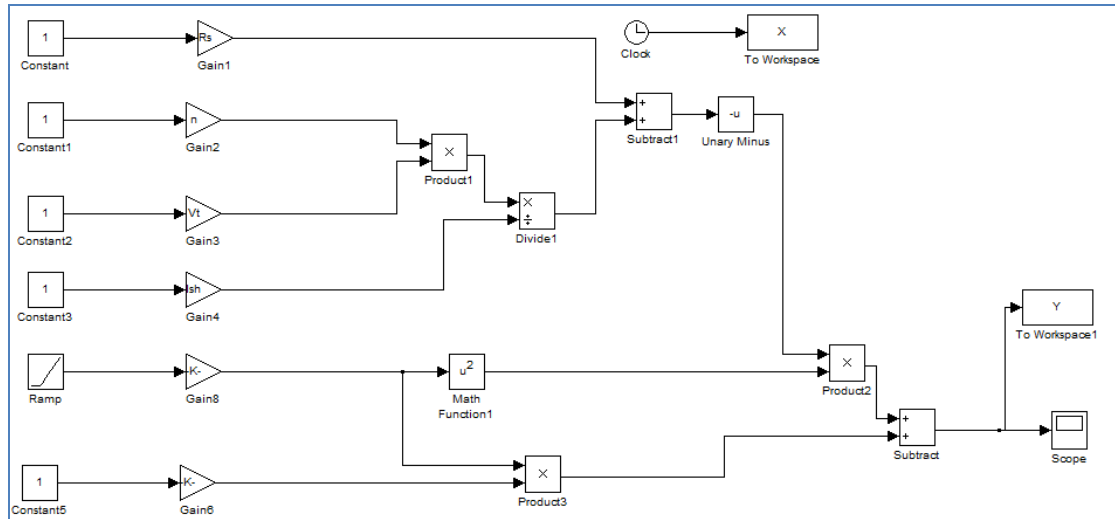


**Fig. (3)** The proposed block diagram model of maximum output power

### 3.4 Fill factor model

Fill factor describes the quality of the current–voltage curve. It is used to compare different solar cells under same reference conditions. It is a measure of junction

quality and series resistance. The closer the FF to unity, the higher the quality of the PV module will be. It is given by [10,12,20].

$$FF = \frac{V_{max} I_{max}}{V_{oc} I_{photo}} = \frac{P_{max}}{V_{oc} I_{photo}} \quad (26)$$

By substituting from Eqs. 9 and 25 in Eq. 26, we get

$$FF = \frac{-\left(R_s + \frac{nV_T}{I_{sh}}\right) I_{max}^2 + V_{oc} I_{max}}{V_{oc} qES \left( \begin{array}{l} \mu_n (\alpha\phi_0 \text{heaviside}(t)+n_0 - \alpha\phi_0 \xi) e^{-\frac{1+Rp_0\tau_{n,t}}{\tau_n}} + \\ \mu_p (\alpha\phi_0 \text{heaviside}(t)+p_0 - \alpha\phi_0 \xi) e^{-\frac{1+Rn_0\tau_{p,t}}{\tau_p}} \end{array} \right)} \quad (27)$$

#### 4. RESULTS AND DISCUSSIONS

Different characteristics of photovoltaic solar cells are calculated in order to analyze the behavior of photovoltaic solar cells under the variation of the most interesting parameters. The reference values of these parameters are shown in Table 1. These values of the calculations are taken from [14,16,17].

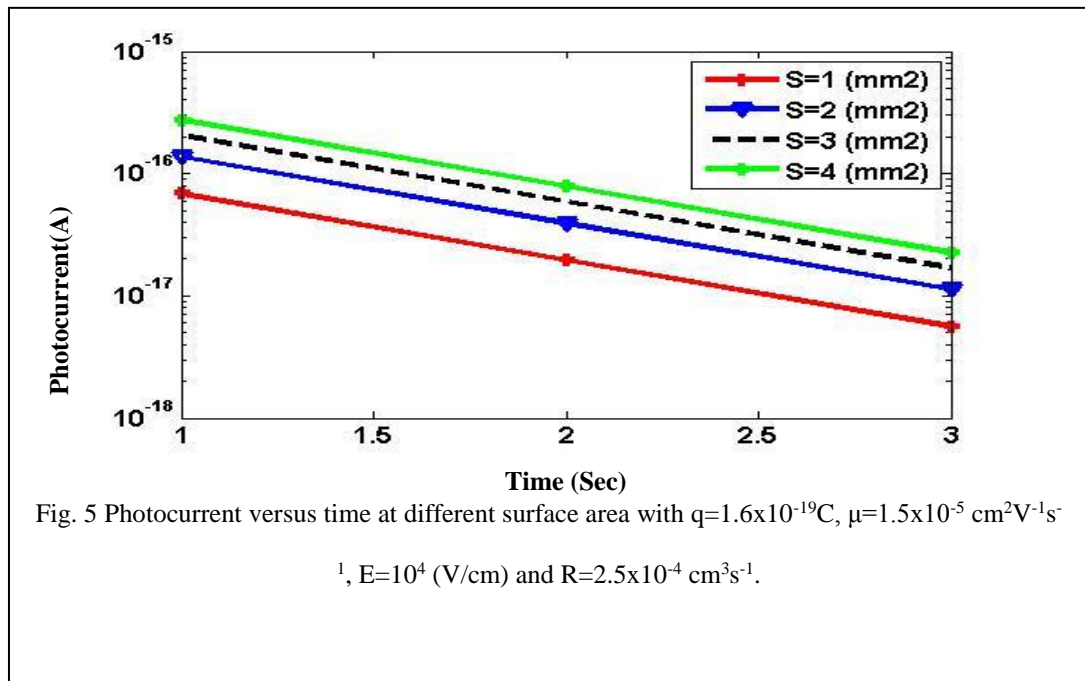
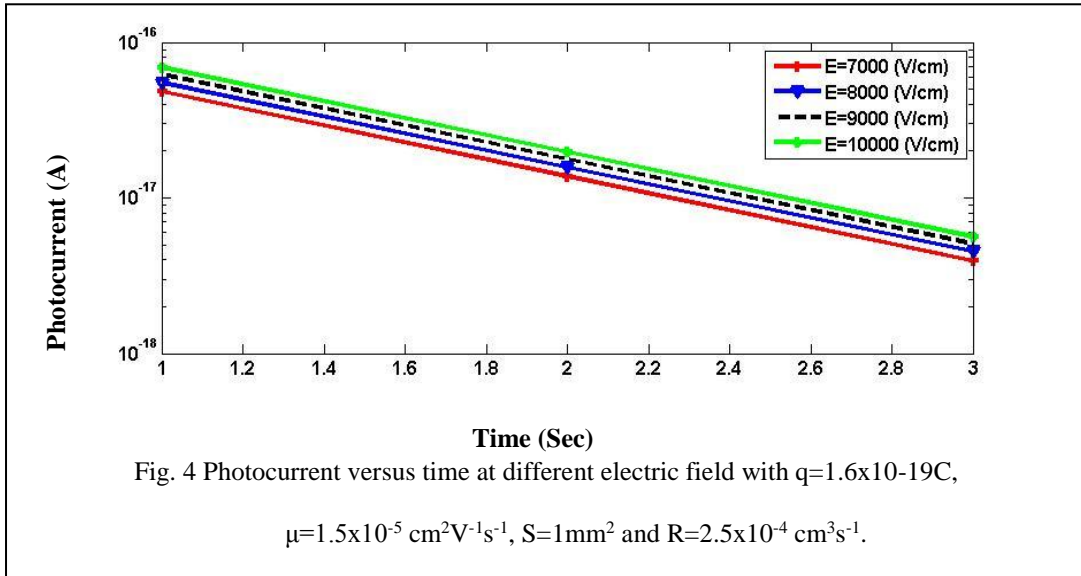
**Table 1** photovoltaic solar cell parameters

T=200-300 K	n(>1)=1.035-1.5	$\tau_p=1 \mu s$	$q=1.6 \times 10^{-19} C$	$E=10^4-10^6 Vcm^{-1}$
$\mu_p=1.5 cm^2V^{-1}S^{-1}$	$\Phi=1000 cm^2S^{-1}$	$\theta=0.95$	$K=1.23 \times 10^{-23} J/K$	$R=2.5 cm^3S^{-1}$
$\mu_n=1.5 cm^2V^{-1}S^{-1}$	$\tau_n=1 \mu s$	$\alpha=0.1 cm^{-1}$	$S=1-2 mm^2$	$R_s=0.0474 \Omega$

##### 4.1 The photocurrent result

The change of photocurrent with time at the different electric field and surface area is shown in Fig. (4) and Fig. (5), respectively. From these figures, the photocurrent decreases with time. The change of the photocurrent with the electric field is depicted in Fig. 4.

We notice that the photocurrent increases with electric field. That is due to the fact that increasing the electric field leads to increasing the amount of absorption of incident photons. However, the change of the photocurrent with the surface area is depicted in Fig. 5. From this figure, the photocurrent increases with surface area. More photons will be absorbed as the surface area, which is directed to the incident radiation, increases. Therefore, the irradiance is increased. Hence, the photocurrent is increased.

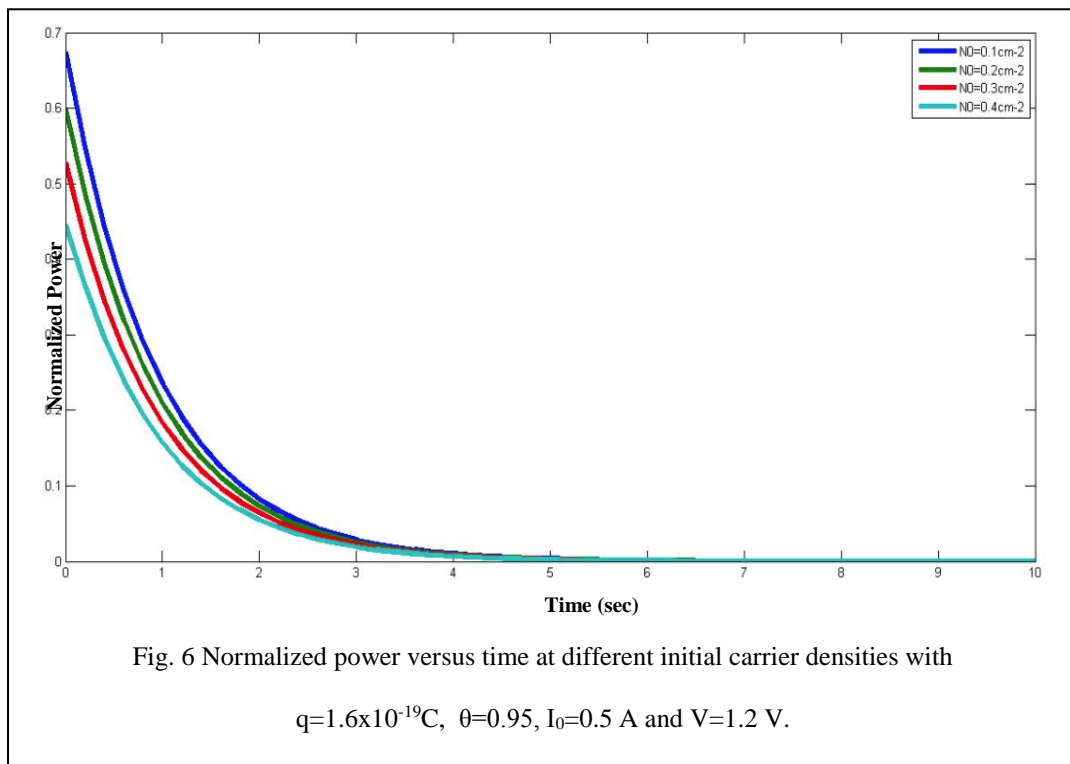


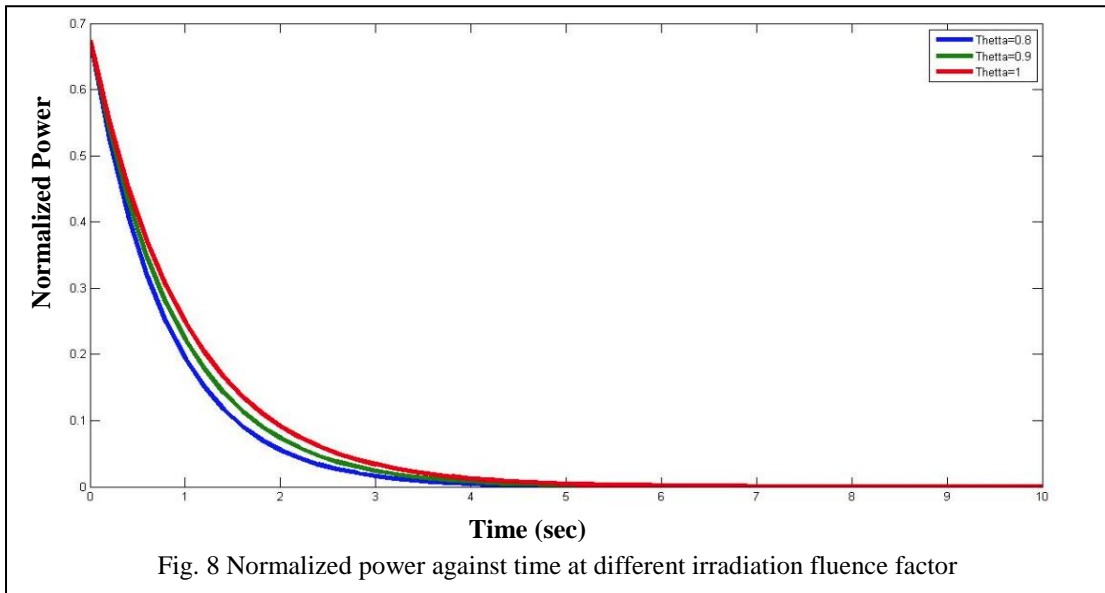
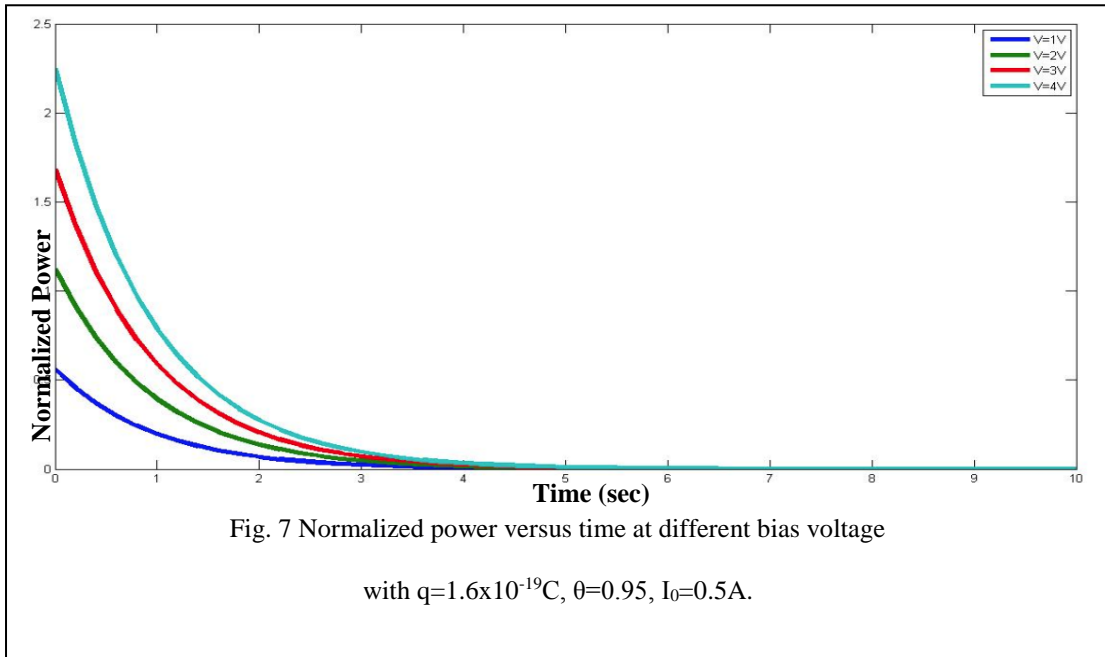
#### 4.2 Output power results

The change of the normalized power with time at different initial carrier densities and bias voltage is shown in Fig. 6 and Fig. 7, respectively. The change of the normalized power ( $P_{\text{out}}/P_{\text{in}}$ ) with initial carrier densities is depicted in Fig. 6. As illustrated in this

figure, the normalized power decreases with initial carrier densities. Since, the input power increases with these carriers. The power ratio ( $P_{out}/P_{in}$ ) decreases. Therefore, the normalized power decreases. The change of the normalized power with bias voltage is illustrated in Fig. 7. From this figure, the input power increases with increasing the bias voltage. Therefore, the power ratio ( $P_{out}/P_{in}$ ) decreases. Thus, the normalized power decreases with increasing the base voltage. The effect of incident radiation fluence on normalized power is shown in Fig. 8. From this figure, the output power increases with incident radiation fluence. Thus, the power ratio increases. On other hand, the normalized power increases with radiation fluence.

As a last point of observation, the output power comes from two different irradiations. The first irradiations are the normal solar irradiations. However, the other one is originated from cosmic rays. Thus, the solar cell structure can be affected.

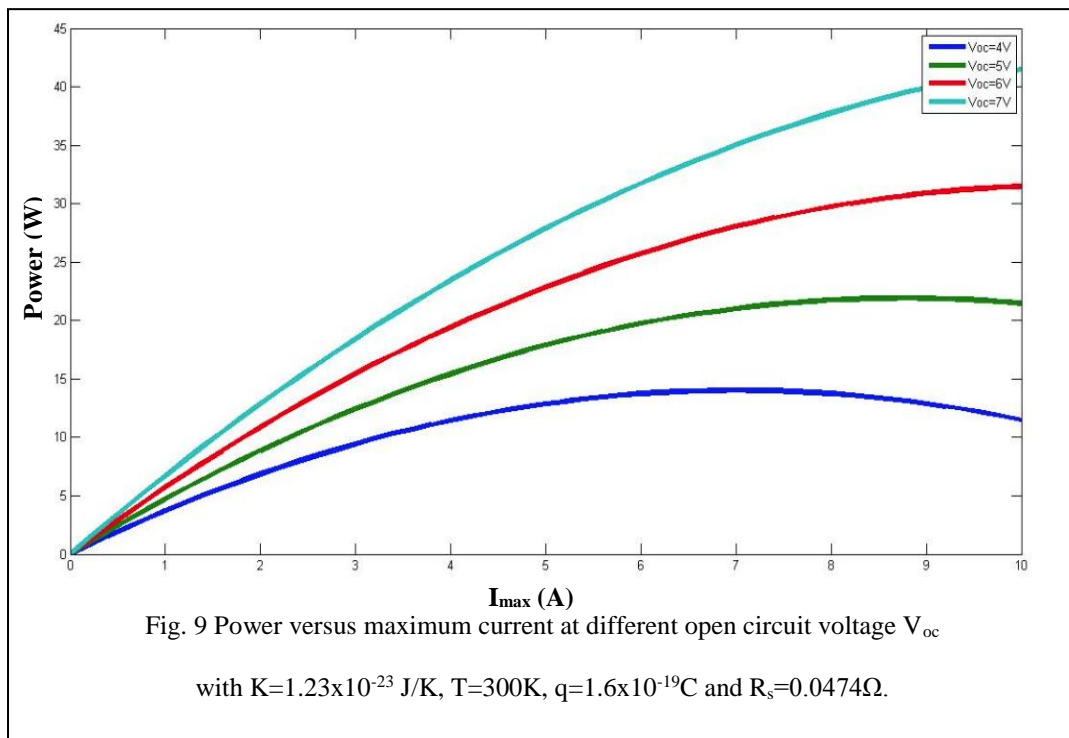


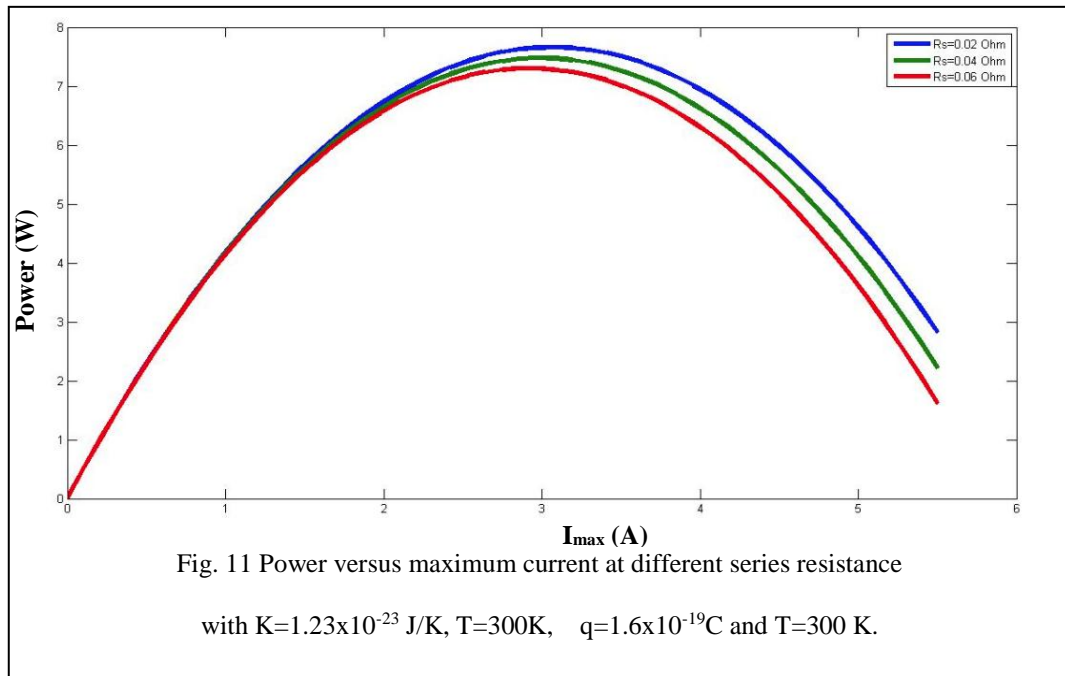
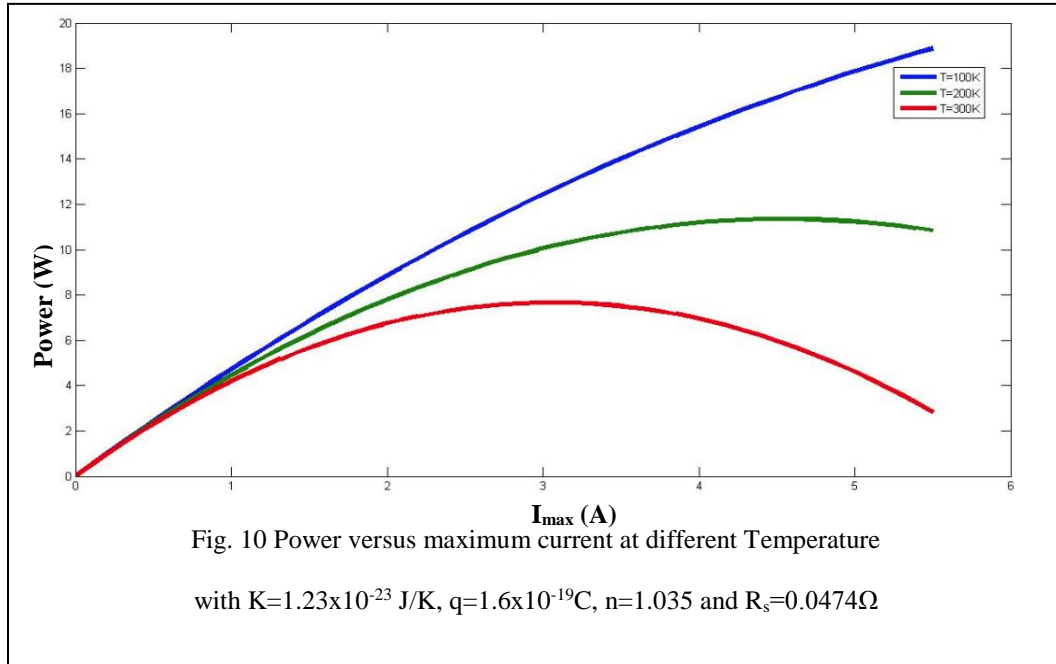


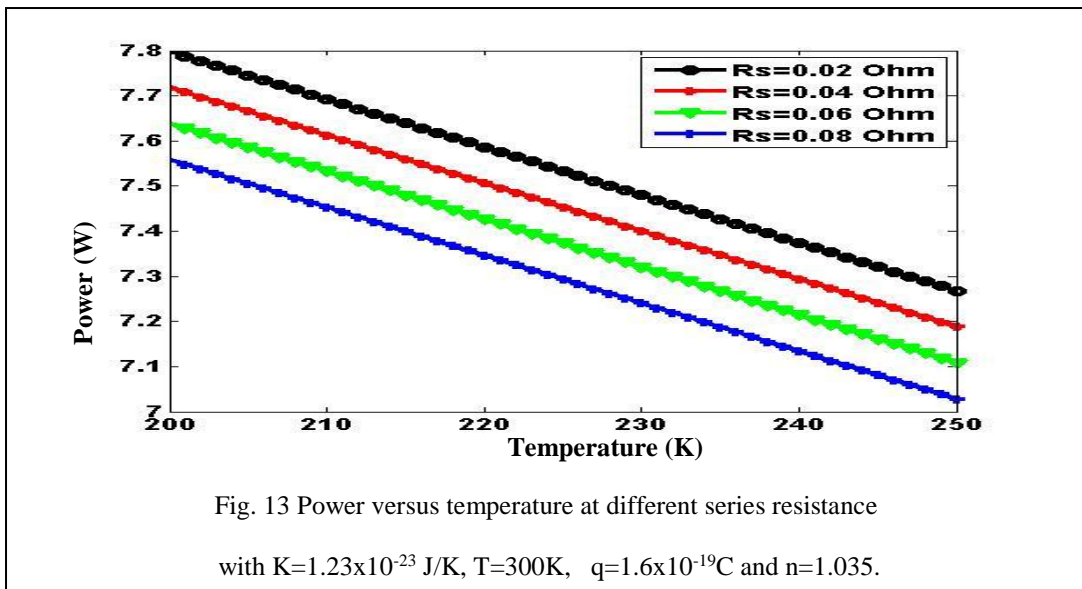
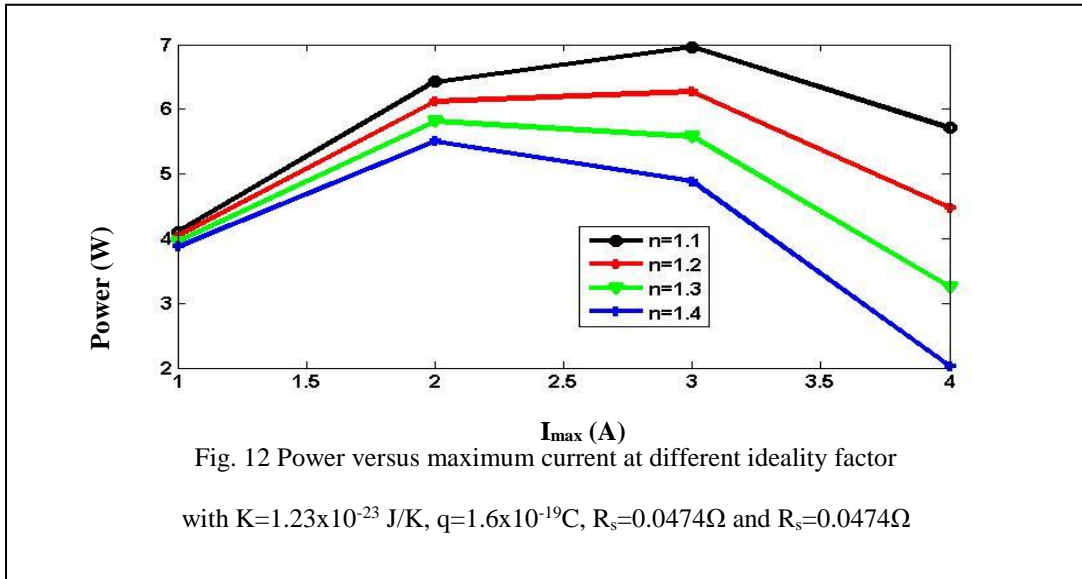
#### 4.3 Maximum output power result

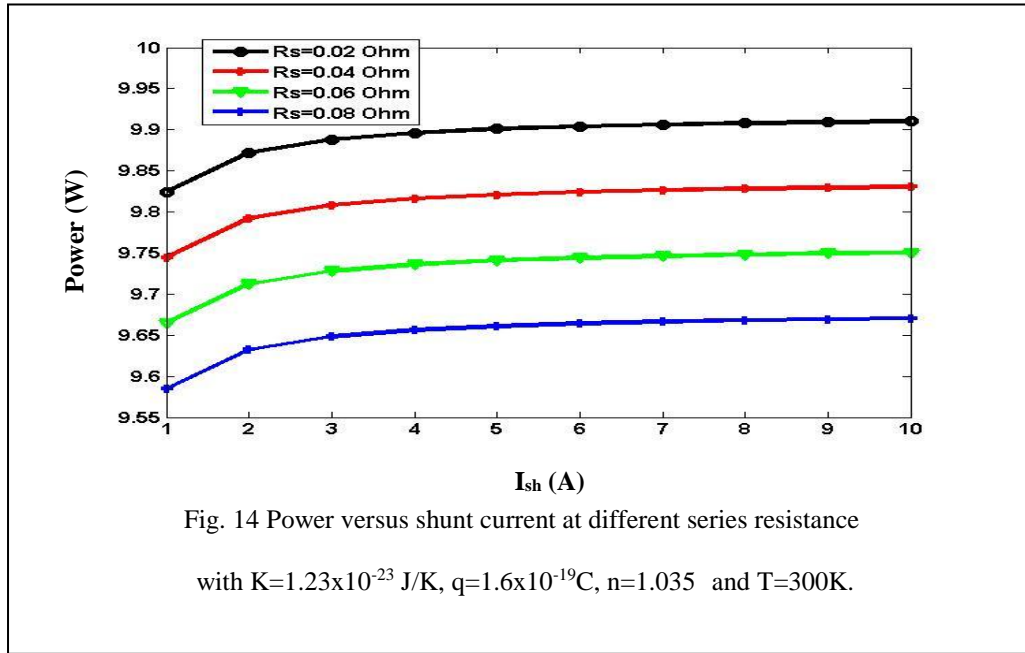
The change of power with maximum current at different open circuit voltage, temperature, series resistance and ideality factor are shown in Figs. 9-11, respectively. The change of the maximum power with open circuit voltage is depicted in Fig. 9. From the figure, the maximum power decreases with open circuit voltage. We noticed that short-circuit current decreases with the increase of open circuit voltage.

Consequently, the output power decreases. The solar cell is a constant current source at low voltages with current that approximately equal to the short circuit current [20]. The current starts to drop off with increases of voltage. Furthermore, there is one point where the cell operates at the highest efficiency that is the maximum power point [20]. The change of the maximum power with temperature is depicted in Fig. 10. As illustrated in this figure, the maximum power increases with the decrease of temperature. Since, the open circuit voltage increases with temperature. Therefore, the short-circuit current decreases. Thus, the maximum power decreases. Also, the change of the maximum power with series resistance is depicted in Fig. 11. The maximum power decreases with increase of series resistance. The short current within the circuit decreases with the increase of series resistance. Therefore, maximum power decreases. Moreover, the change of the maximum power with ideality factor is depicted in Fig. 12. The corresponding maximum power decreases with the ideality factor. A higher value of ideality factor is attributed to inhomogeneous barrier and recombination of electrons and holes in the depletion region [14]. Therefore, minority carriers are photo-excited. Thus, the obtained output power decreases. However, the ideal diode behavior is corresponding to ideality factor value of 1. The change of the power with the temperature at different series resistance is shown in Fig. 13. From this figure, the power decreases with both temperature and series resistance. However, the change of the power with shunt current at different series resistance is depicted in Fig. 14. The parasitic from p-n junction is reduced with the increase of shunt current. Therefore, the output power increases. But, the overall parasitic is not completely avoided. Thus, saturation of the power is deduced as illustrated in the figure.



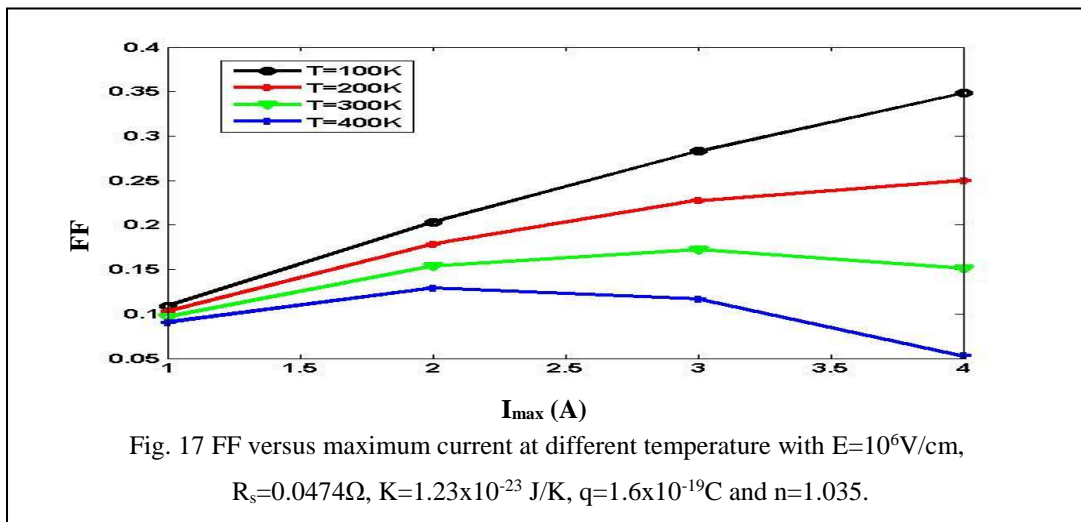
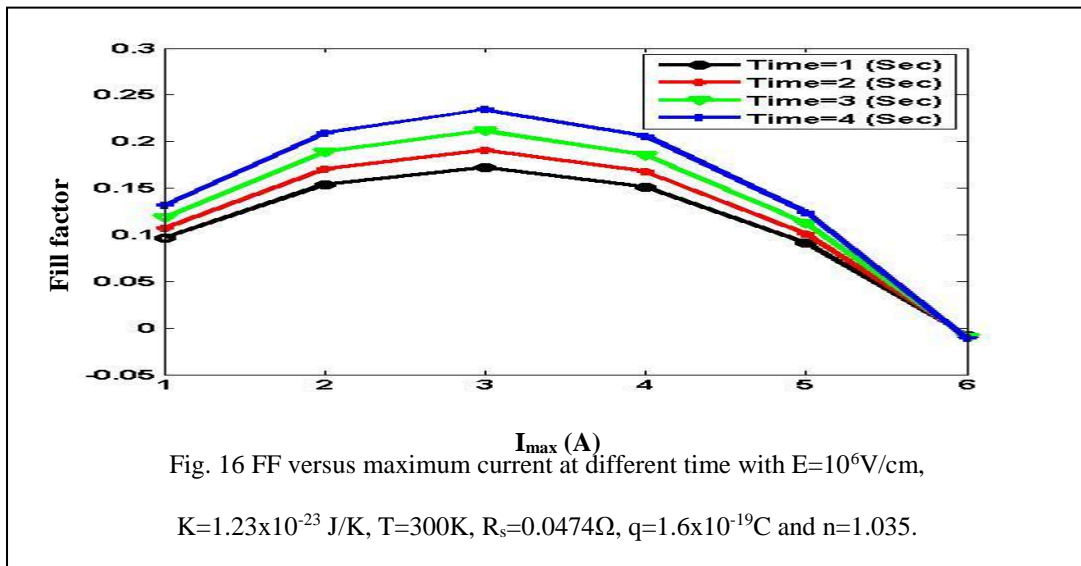
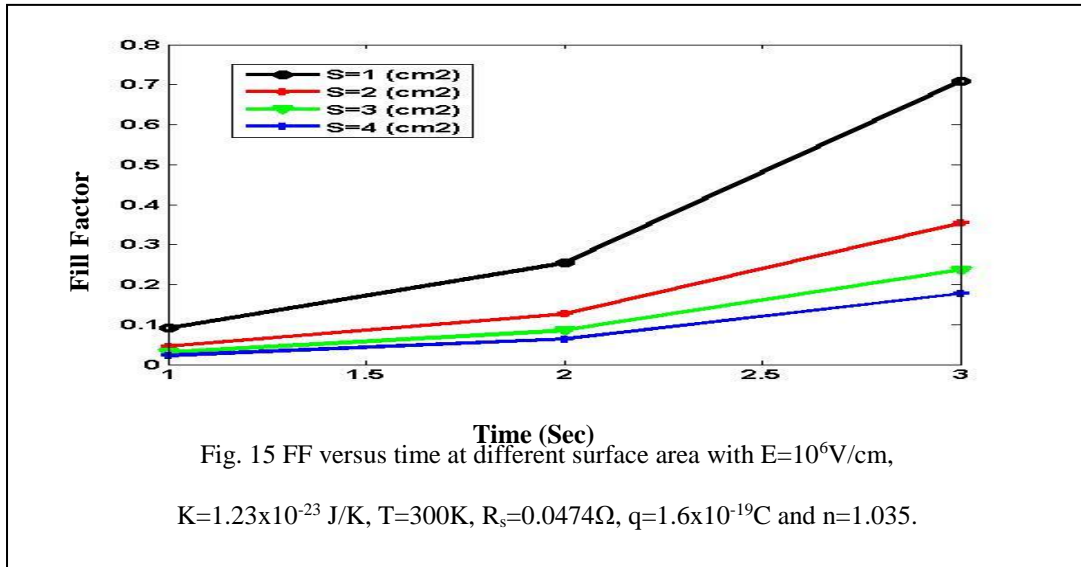


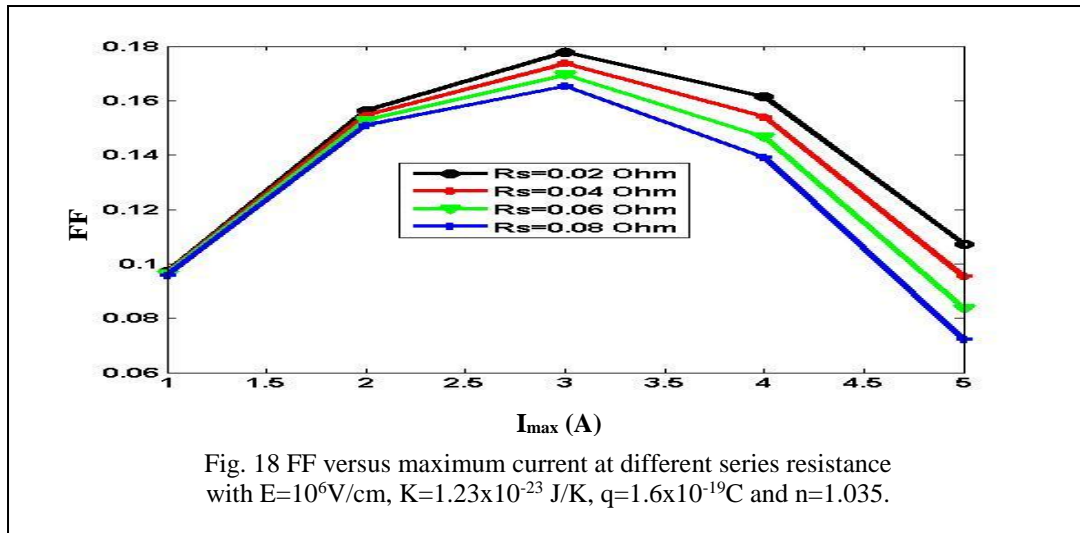




#### 4.4 Fill factor result

The change of the fill factor with time at the different surface area is shown in Fig. 15. From this figure, the fill factor decreases with surface area. We noted that as the surface area is increased. The absorption of the incident photons is increased. The output power is increased. Thus, the fill factor is decreased. The change of the fill factor with maximum current at the different time, temperature, and series resistance are shown in Figs. 16-18, respectively. The change of the fill factor with time is depicted in Fig. 16. As we noted from this figure, the maximum behavior was achieved at the maximum current of 3A. The change of the fill factor with temperature is depicted in Fig. 17. The output power decreases with temperature. So, the fill factor increases. The change of the fill factor with series resistance is depicted in Fig. 18. The maximum power decreases with the increase of series resistance. Therefore, the fill factor increases with series resistance.





## CONCLUSION

Analysis and evaluation of photovoltaic solar cells under high radiation effects is the target of this manuscript. Thus, implicit and explicit solutions of solar cells behaviors are presented. These solutions depend on four parameter model of the cell with photocurrent source, a parallel diode, parallel shunt resistance and a series resistor. Explicit models using MATLAB environment is proposed. However, implicit solution based on a block diagram models are implemented. These models have the advantageous of simplicity and easy of tuning. Moreover, the block diagram models helps manufacture and scientists to optimize solar cells characteristics. These characteristics are photocurrent, output power, maximum output power and fill factor. Several performance parameters are tuned to enhance the performance of solar cells through the presented methodology. On other hand, using of graphical user interface by MATLAB SimuLink allows a quick experimentation with alternative values of performance parameters such as electric field, surface area, bias voltage and temperature. The results show that optimum output power of 1.68611235 Watt per cell is achieved. Also, the cell surface area and series resistance have a strong effect on the cell behaviors that must be carefully chosen.

## REFERENCES

- [1] A. Ganguly, D. Misra, and S. Ghosh, "Modeling and analysis of solar photovoltaic-electrolyzer-fuel cell hybrid power system integrated with a floriculture greenhouse", *Energy and Buildings*, Vol. 42, pp. 2036–2043, 2010.

- [2] Hegazy Rezk, and Abou Hashema M. El-Sayed, "Sizing of a stand alone concentrated photovoltaic system in Egyptian site", *Electrical Power and Energy Systems*, Vol. 45, pp. 325–330, 2013.
- [3] M. Petit, T. Ethvignot, T. Granier, R.C. Haight, J. M. O. Donnell, D. Rochman, S.A. Wender, E. M. Bond, T. A. Bredeweg, D. J. Vieira, J. B. Wilhelmy, and Y. Danon, "A compensated fission detector based on photovoltaic cells", *Nuclear Instruments and Methods in Physics Research A*, Vol. 554, pp. 340–346, 2005.
- [4] M. Valan Rajkumar, and P.S. Manoharan, "FPGA based multilevel cascaded inverters with SVPWM algorithm for photovoltaic system", *Solar Energy*, Vol. 87, pp. 229–245, 2013.
- [5] Rodolphe Vaillon, Lucile Robin, Cristian Muresan, and Christophe Menezo, "Modeling of coupled spectral radiation, thermal and carrier transport in a silicon photovoltaic cell", *International Journal of Heat and Mass Transfer*, Vol. 49, pp. 4454–4468, 2006.
- [6] Kashif Ishaque, Zainal Salam, Amir Shamsudin, and Muhammad Amjad, "A direct control based maximum power point tracking method for photovoltaic system under partial shading conditions using particle swarm optimization algorithm", *Applied Energy*, Vol. 99, pp. 414–422, 2012.
- [7] Nejib Hamrouni, Moncef Jraidi, and Adnene Cherif, "Theoretical and experimental analysis of the behavior of a photovoltaic pumping system", *Solar Energy*, Vol. 83, pp. 1335–1344, 2009.
- [8] S. Aydogan, and A.Turut, "Influence of 12 MeV electron irradiation on the electrical and photovoltaic properties of Schottky type solar cell based on carmine", *Radiation Physics and Chemistry*, Vol. 80, pp. 869–875, 2011.
- [9] M. Alurralde, M.J.L. Tamasi, C. J. Bruno, M. G. Martnez Bogado, J. Pla, J. Fernandez Vazquez, J. Duran, J. Schuff, A. A. Burlon, P. Stoliar, and A. J. Kreiner, "Experimental and theoretical radiation damage studies on crystalline silicon solar cells", *Solar Energy Materials and Solar Cells*, Vol. 82, pp. 531–542, 2004.
- [10] M. Ashry, and S.A. Fayek, "Radiation effects on fabricated Cu<sub>2</sub>S/CdS heterojunction photovoltaic cells", *Renewable Energy*, Vol. 23, pp. 441–450, 2001.
- [11] M. Y. Feteha, "Gamma radiation effect on the GaAs solar cell performance", *IEEE International Symposium on Compound Semiconductors*, pp. 91-96, 2000.
- [12] L. El Chaar, L.A. lamont, and N. El Zein, "Review of photovoltaic technologies", *Renewable and Sustainable Energy Reviews*, Vol. 15, pp. 2165–2175, 2011.

- [13] Vivek Tamrakar ,S.C. Gupta and Yashwant Sawle, "Single-diode and two-diode pv cell modeling using matlab for studying characteristics of solar cell under varying conditions", *Electrical and Computer Engineering: An International Journal (ECIJ)*, Vol. 4, No. 2, pp. 67-77, 2015
- [14] R. Chenni, M. Makhlouf, T. Kerbache, and A. Bouzid, "A detailed modeling method for photovoltaic cells", *Energy*, Vol. 32, pp. 1724–1730, 2007.
- [15] N. Loussaef, L. Hassine, N. Boutabba, F. Kouki, P. Spearman, F. Garnier and H. Bouchriha, "Theoretical and experimental study of photocurrent action spectrum of ITO/sexithiophene/Al structure", *Synthetic Metals*, Vol. 128, pp. 283–287, 2002.
- [16] N. Boutabba, L. Hassine, A. Rihani, and H. Bouchriha, "Analytic photocurrent transient response of an Al/6T/ITO photovoltaic cell using Volterra series analysis", *Synthetic Metals*, Vol. 139, pp. 227–231, 2003.
- [17] Zhenyu Hu, Shiyu He, and Dezhuang Yang, "Effect of <200 keV proton radiation on electric properties of silicon solar cells at 77 K", *Nuclear Instruments and Methods in Physics Research B*, Vol. 217, pp. 321–326, 2004.
- [18] Carlos R. Sanchez Reinoso, Diego H. Milone, and Roman H. Buitrago, "Simulation of photovoltaic centrals with dynamic shading", *Applied Energy*, Vol. 103, pp. 278–289, 2013.
- [19] J. I. Rosell, and M. Ibanez , "Modelling power output in photovoltaic modules for outdoor operating conditions", *Energy Conversion and Management*, Vol. 47, pp. 2424–2430, 2006.
- [20] K. H. Lam, T. M. Lai, W. C. Lo, and W. M. To, "The application of dynamic modelling techniques to the grid-connected PV (photovoltaic) systems", *Energy*, Vol. 46, pp. 264-274, 2012.